Drug Development and Industrial Pharmacy, 2009; 35(11): 1348–1355

informa
healthcare

ORIGINAL ARTICLE

Preparation and evaluation of *N*-caproyl chitosan nanoparticles surface modified with glycyrrhizin for hepatocyte targeting

AiHua Lin[1], Jun Chen[2], YiMing Liu[1], Shigui Deng[1], Zhifeng Wu[1], Yu Huang[1] and QiNeng Ping[3]

[1]*Pharmaceutics Laboratory of TCM, The Second Faculty of Clinical Medicine, Guangzhou University of Chinese Medicine, Guangzhou, Guangdong, PR China,* [2]*School of Pharmacy, Nanjing University of Chinese Medicine, Nanjing, Jiangsu, PR China and* [3]*Department of Pharmaceutical Technology, Faculty of Pharmacy, China Pharmaceutical University, Nanjing, Jiangsu, PR China*

Abstract

Background: The development of an efficient targeted drug delivery system into cells is an important subject for the advancement of drug carriers. In this study, a novel hepatocyte-targeted delivery system with glycyrrhizin (GL) surface modification based on *N*-caproyl chitosan (CCS) has been developed. *Method*: CCS was synthesized by acylation of amino group of chitosan, and GL was oxidized to be conjugated to the surface of *N*-caproyl chitosan nanoparticles (CCS-NPs-GL). The synthesized nanoparticles were first characterized for their morphology, particle size, zeta potential, in vitro stability in plasma, tissue distribution, and hepatocyte-targeting uptake in vivo. *Results*: The obtained results showed that the spherical and discrete nanoparticles prepared with oxidized GL/CCS ratio of 0.14:1 (w/w) exhibited a positive electrical charge and associated adriamycin quite efficiently (association efficiency: 87.5%). The prepared nanoparticles also possessed dimensional and GL surface-binding stability and slow release property in plasma in vitro. The biodistribution of these particles after intravenous injections in mice revealed accumulating drug concentrations in the liver, spleen, and lungs while decreasing drug concentrations in the heart and kidney. The content of adriamycin-loaded CCS-NPs-GL in the liver was 1.6 times higher than that of non-GL-modified CCS-NPs. Furthermore, in vivo uptake of CCS-NPs-GL by rat hepatocytes showed 2.1 times higher nanoparticle uptake compared with non-GL-modified CCS-NPs, which suggested that CCS-NPs-GL were preferentially distributed in hepatocytes by a ligand–receptor interaction. *Conclusion*: This article indicated that CCS-NPs-GL was a stable and effective drug delivery vehicle for hepatocyte targeting.

Key words: *Glycyrrhizin; hepatocyte-targeting; nanoparticle; N-caproyl chitosan; surface modification; tissue distribution*

Introduction

Targeted drug delivery is under extensive development to increase drug concentration in the required sites without side effects on normal tissues. In recent years, different new drug carrier systems in the micro- and nanometer size range were generated for this purpose. Among various drug carrier systems, nanoparticles have certain advantages over other delivery systems such as a maximal load of the drug and a long shelf life[1]. Furthermore, their body distribution and permeability in tissues can be controlled by size and surface properties as well as by the attachment of targeting ligands[2,3].

Chitosan is a cationic polysaccharide obtained by partial deacetylation of chitin, the major component of crustacean shells. Chitosan nanoparticles prepared by ionic gelation method have a special role in drug delivery for use in medical or pharmaceutical applications because of its biocompatibility, biodegradability, increased transfection efficiency, and low toxicity[4–6]. However, this system is significantly limited by its low cell specificity.

Address for correspondence: Dr. AiHua Lin, PhD, Pharmaceutics Laboratory of TCM, The Second Faculty of Clinical Medicine, Guangzhou University of Chinese Medicine, Guangzhou, Guangdong 510120, PR China. E-mail: linah76@163.com

(Received 24 Sep 2008; accepted 1 Apr 2009)

ISSN 0363-9045 print/ISSN 1520-5762 online © Informa UK, Ltd.
DOI: 10.3109/03639040902939197

To overcome this, several ligands, such as transferring-[5], folate-[7], mannose-[8], and galactose[9]-conjugated chitosan, have been designed for receptor-mediated endocytosis drug delivery. Of the ligand-conjugated chitosans, glycyrrhizin (GL) surface modification has been proved to be an efficient access to increase hepatic targeting[10]. GL, used as a treatment for chronic viral hepatitis, is one of the main compounds extracted from the root of *Glycyrrhiza glabra* (licorice). In 1990s, Negishi et al.[11] proved that there are specific binding sites of GL on the cellular membrane of in vitro rodentine hepatocytes. In recent years, Ismair et al.[12] have found that carrier-mediated transport system participates in the uptake of GL into rat and human hepatocytes. These researches imply that GL may be used as a novel ligand for hepatocyte-specific delivery.

It was previously reported by our group that GL-modified chitosan nanoparticles were preferentially accumulated in hepatocytes in vitro due to the specific ligand–receptor interactions[13–15]. However, in some fields, especially in medicine and pharmaceutical industry, the application of chitosan nanoparticles prepared by ionic gelation method is limited by its instable characteristic in physiological pH condition, resulting in particle aggregation because of the strong inter- and intramolecular hydrogen bonding[16,17]. It is unsuitable for cell- and tissue-targeted delivery in vivo by intravenous (i.v.) administration. It has been reported that the N-acylation of chitosan with fatty chain groups can induce a hydrophobic nature to reduce molecular hydrogen bonding and increase stabilization of chitosan by hydrophobic interactions[18].

Therefore, in this study, especially increasing particle stability in physiological pH condition for i.v. administration was focused. For this purpose, *N*-caproyl chitosan (CCS) was synthesized by acylation of amino group, and GL surface-modified CCS nanoparticles (CCS-NPs-GL) were prepared by periodate oxidation method. The nanoparticles obtained were first characterized for their morphology, particle size, zeta potential, AE, and in vitro stability in plasma. Finally, their tissue distribution and hepatocyte-targeting uptake in vivo were also evaluated.

Materials and methods

Materials and animals

Chitosan (CS, deacetylation degree >85%), GL, and poly(vinyl sulfate kalium salt) were purchased from Sigma (St. Louis, MO, USA). Caproic anhydride was purchased from Shanghai Jiachen Chemical industrial Limited Company (Shanghai, China). Pentasodium tripolyphosphate (TPP) was supplied by Tianjin Chemical Company (Tianjin, China). Adriamycin·HCl (ADR·HCl) was obtained from Haizhen Pharmaceutical Limited Company (Zhejiang, China). Sodium periodate was purchased from Shanghai Chemical Reagent Limited Company (Shanghai, China). Methanol and acetonitrile were chromatographic pure. All the other reagents were of analytical grade and used without further purification.

Wistar rats (range, 180–220 g) and Kunming strain mice (range, 20–30 g), from the Central Animal House of the Guangzhou University of Traditional Chinese Medicine (Guangzhou, Guangdong, China), were used. They were kept in a 12-hour light–dark cycle and at a temperature of 20 ± 2°C. The animals were allowed access to food and water ad libitum.

Synthesis of CCS

Chitosan N-acylation was performed by the method of Lee[17]. Two grams of chitosan were dissolved in 100 mL of 1% aqueous acetic acid solution and 100 mL of methanol was added dropwise under 1000 rpm agitation. Then, 50 mL of 2% caproic anhydride solution in methanol was added to the chitosan solution. After 4 hours, the chitosan solution was poured into the same volume of methanol: 0.1 mol/L NaOH (7:3, v/v). The precipitated chitosans were filtered, washed thoroughly with methanol and ether, and then dried in a vacuum at 50°C.

Preparation of CCS-NPs and CCS-NPs-GL

According to the procedure previously developed by our group[13,14], CCS-NPs were formed spontaneously upon addition of an aqueous TPP solution (0.8 mg/mL) to CCS solution (2 mg/mL, dissolved in 1% acetic solution) at volume ratio of 2:5 under magnetic stirring. ADR (as a model drug)-loaded nanoparticles were formed upon incorporation of TPP solution into CCS solution containing 0.4 mg/mL ADR at the same ratio.

CCS-NPs-GL were prepared by periodate oxidation method as described elsewhere[15]. Briefly, GL (0.1 mol/L) was oxidized by sodium periodate (0.1 mol/L) at the same volume. Then, 80% methanol was added to remove the sediment. The oxidized GL was lyophilized by a freeze drier (Alpha 1-2; Christ, Osterode am Harz, Germany) to obtain the dried oxidized GL. Finally, different contents of oxidized GL (dissolved in distilled water) were added dropwise into the nanoparticles suspension at oxidized GL/CCS ratio of 0.14:1 (w/w) under magnetic stirred conditions for 6 hours.

Characterization of CCS

Fourier transform infrared (FTIR) spectra of CS and CCS were measured as KBr pellets using an Avatar 360IR spectrophotometer (Nicolet Company, Madison, WI, USA). ^{1}H-NMR spectra of CS and CCS were measured in D_2O containing a small amount of CD3COOD using an Inova

500NB (Varian Company, Palo Alto, CA, USA). The fraction of substituted amino groups (degree of substitution) was done by colloidal titration[15]. Degree of substitution was calculated according to the following equation:

$$\text{Degree of substitution } (\alpha) = \frac{\Delta V_{CS} - (161 + 98\alpha)\cdot \Delta V_{CCS}/161}{\Delta V_{CS}} \times 100\%, \quad (1)$$

where ΔV_{CS} and ΔV_{CCS} are the net consumed volume of PVSK standard solution in the titration of CS and CCS solution, respectively. 161 is element M_W of CS, 98 is M_W of $-CO(CH_2)_5$.

Equation (1) is rearranged with the following equation:

$$\text{Degree of substitution } (\alpha) = \frac{\Delta V_{CS} - \Delta V_{CCS}}{\Delta V_{CS} + 0.609\Delta V_{CCS}} \times 100\%. \quad (2)$$

Characterization of nanoparticles

Particle morphology was examined by transmission electron microscopy (JEM-2010HR; JEOL, Tokyo, Japan). One drop of nanoparticle suspension was placed on a copper grid and stained with 2% phosphotungstic acid solution for 2 minutes. The grid was allowed to dry at room temperature and was examined with the electron microscope.

The particle size and zeta potential of nanoparticles were assessed, respectively, by dynamic light scattering (DLS) and laser Doppler anemometry using a Zetasizer 3000 (Malvern Instruments, Malvern, UK). The nanoparticle suspension was filtered with a 0.45-μm filter, and each batch was analyzed in triplicate.

Drug content encapsulated in nanoparticles was measured by high-performance liquid chromatography (HPLC) developed previously by our group[15]. Briefly, the ADR-loaded nanoparticles were separated from the aqueous medium by ultrafiltration (3000 M_W; Sartorius, Hannover, Germany) at 3000 rpm for 15 minutes. The amount of free ADR in the centrifugate was measured by HPLC. The ADR AE was calculated according to the following equation:

$$\text{AE} = \frac{\text{total ADR} - \text{tree ADR}}{\text{total ADR}} \times 100\%.$$

Nanoparticle stabilization and in vitro release of ADR from nanoparticles in plasma

To study stabilization and in vitro release characterization in human plasma, 20 mL of nanoparticles suspension was incubated with 100 mL of human plasma for different incubation times at 37°C. At appropriate time, 3 mL of plasma was removed and the same volume of blank plasma was added into the system. The particle size was assessed by DLS. The amount of glycyrrhetic acid, an aglycone of oxidized GL, hydrolyzed by 5% sulfuric acid, was determined by HPLC[13,14], and ADR in the plasma medium was measured by liquid chromatography–tandem mass spectrometry (LC/MS/MS) method described as below. Surface GL-binding ratio was calculated according to the following equation:

$$\text{Surface GL-binding ratio} = \frac{\text{total oxidized GL} - \text{free oxidized GL}}{\text{total oxidized GL}} \times 100\%.$$

In vivo tissue distribution of the nanoparticles

In vivo testing protocol was approved by the Animal Ethics Committee of Guangdong Provincial Hospital of TCM. The Kunming strain mice were intravenously injected with the same dose of ADR in the three different formulations (15 mg/kg in mice for each drug formulation: ADR solution, ADR-loaded CCS-NPs suspension, and ADR-loaded CCS-NPs-GL suspension). Blood was collected by eye puncture after general heparinization, and the mice were killed at 15 minutes, 1, 2, 4, 8, and 24 hours after the injection ($n = 6$ at each time point) to collect samples of liver, spleen, kidney, heart, and lung. The plasma was separated by centrifugation at 2095 × *g* for 5 minutes. The cardiac tissue was sectioned and blotted with lint-free paper toweling to remove residual blood. No attempt was made to remove blood from other tissues. The tissues such as the heart, liver, spleen, lung, and kidney were weighed and homogenized in normal saline using tissue homogenizer (6000 rpm) at the cold-bath condition. All plasma samples and tissue homogenates were labeled and placed into polypropylene cryovials and immediately frozen at –80°C until analysis.

The analysis of ADR in plasma and tissues

The concentration of ADR in plasma and tissue was determined by a validated HPLCLC/MS/MS method. Daunorubicin was selected as the internal standard (IS). To each 200-μL tissue homogenate or plasma sample, 40 μL of IS solution (800 ng/mL) was added. After vortex-mixing for 10 seconds, 2 mL chloroform–methanol (4:1, v/v) was added; the mixture was vortexed for 3 minutes. Following centrifugation (3000 rpm, 15 minutes) and separation, the organic phase was transferred, evaporated to dryness, reconstituted with 150 μL of mobile phase, and then 10 μL was

injected for analysis. The analytes were separated on a Pinnacle II C_{18} column (150 × 2.1 mm i.d., 5 µm; Restek, Bellefonte, PA, USA) by isocratic elution with acetonitrile: 10 mmol/L ammonium acetate : acetic acid (70:30:1, v/v/v) at a flow rate of 220 µL/min and quantified using positive ion mode by an API 3000 triple-quadrupole mass spectrometric instrument (Applied Biosystems, Foster City, CA, USA). The fragmentation transitions for the multiple reaction monitoring were m/z 544.2 → 397.2 for ADR and m/z 528.2 → 321.3 for IS.

Targeting analysis

The targeting effect of CCS-NPs-GL system was evaluated by area under curve (AUC) in a certain organ or tissue and targeting index (TI) as described below[19]:

$$TI = \frac{(AUC_i)_{TDDS}}{(AUC_i)_{CDDS}},$$

where $(AUC_i)_{TDDS}$ represents AUC in a certain organ or tissue of targeting drug delivery system, $(AUC_i)_{CDDS}$ represents AUC in a certain organ or tissue of conventional drug delivery system.

In vivo hepatic cellular uptake of CCS-NPs-GL

ADR (10 mg/kg) in CCD-NPs or CCS-NPs-GL suspension was intravenously injected into rats, and the liver specimens were collected 1 hour after the injection. Rat hepatocytes were isolated by the procedure previously described elsewhere[15,20]. Finally, the isolated hepatocytes were transferred at a density of 2×10^6 cell/mL into the tubes and immediately placed in ice. The intracellular fluorescence intensity of ADR (λ_{Ex} = 488, λ_{Em} = 575) was determined on a Beckman Coulter EPICS XL-ELITE flow cytometry (Beckman Coulter Limited, Buckinghamshire, UK) using XL EXPO^{TM}2.0 software. Approximately 5000 event cells were evaluated to determine the trend of hepatocyte targeting. All samples were repeated three times. Between-group intracellular fluorescence intensity of ADR was compared using student's t-test. The null hypothesis was rejected at $P < 0.05$.

Results and discussion

Characterization of CCS

FTIR spectra of both native and CCS are presented in Figure 1. The spectrum of CS exhibited the characteristic amide bands at 1651 cm (amide I) and 1595 cm^{-1} (primary amine band). After N-caproylation, a prominent band at 1555 cm^{-1} (amide II band) was observed. In addition, the intensity of peaks at 2860–2930 cm^{-1} ($-CH_2-$) was increased, which confirmed that the chitosan was substituted by caproyl chain. Furthermore, the broad band (H-banded N–H and O–H) at 3300–3500 cm^{-1} reached an intense peak, indicating lower H-bonding after chemical modification[21].

The ^{1}HNMR spectra of both native and CCS are shown in Figure 2. For CS, peaks at 2.0 ppm could be ascribed to the three N-acetyl protons ($-(CO)-CH_3$) of CS, and at 3.0 ppm to a H_2 proton of CS. Peaks at 3.4–3.8 ppm were considered to H_3–H_6 protons of CS[18]. After modification, new peaks at 0.8, 1.1, and 1.8 ppm were ascribed, respectively, to CH_3, $-CH_2-$, and $-CH_2-(CO)$ of the caproyl residue. About 26.9% of substitution degree was achieved by colloidal titration.

Characterization of nanoparticles

Preliminary experiments were performed to determine the optimal condition for nanoparticle formation. CCS nanoparticles were formed spontaneously upon the

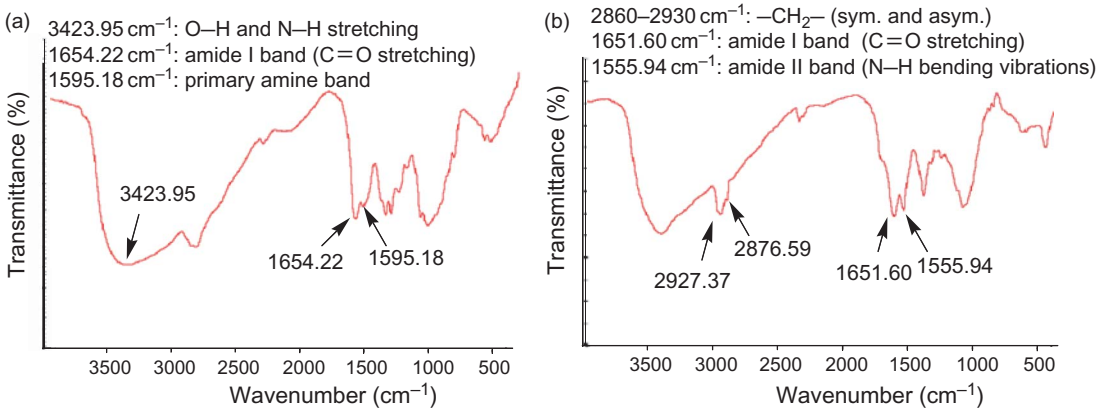

Figure 1. IR spectra of chitosan (a) and *N*-caproyl chitosan (b).

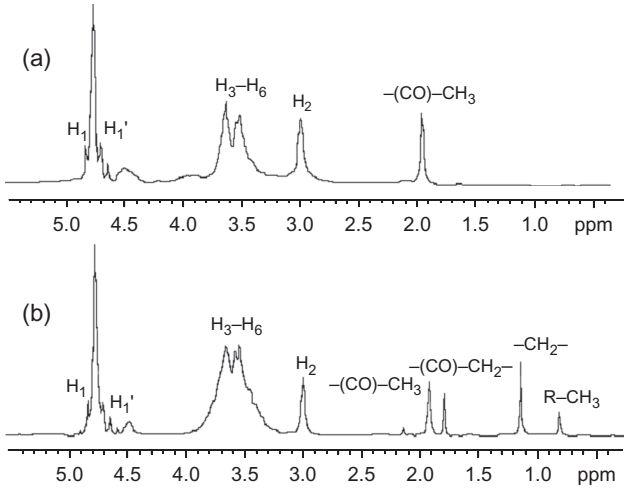

Figure 2. ^{1}HNMR spectra of chitosan (a) and *N*-caproyl chitosan (b).

incorporation of TPP solution to the CCS solution with the fixed CCS/TPP ratio of 6.25:1 (w/w). Then GL was oxidized by periodate oxidation and reacted with residual amino groups on the surface of CCS nanoparticles. The particle size, zeta potential, and drug AE of nanoparticles prepared with different proportions of oxidized GL/CCS are presented in Table 1. The results demonstrated that the mean diameters of particles decreased at first (in pH 6.0 medium) and then increased with oxidized GL/CCS ratio, which can be explained by swelling/shrinking property and inter- and intramolecular linkage of nanoparticles[22]. Because $-NH_3^+$ density on the surface of nanoparticles was responsible for the measured positive zeta potential values, the positive zeta potential stepped down with oxidized GL/CCS ratio, which decreased $-NH_3^+$ density.

It is also interesting to find that GL surface-modification increases encapsulation efficiency of nanoparticles as presented in Table 1. The increase may be due to molecular structure of ADR·HCl, containing ionizable groups. The electrostatic interactions between negative groups of oxidized GL and the positive groups of ADR·HCl may play a role in association of more amount of free ADR from CCS solution to nanoparticles[15].

Table 1. Characterization of nanoparticles with the oxidized GL/CCS ratio (w/w) (mean ± SD, $n = 3$).

Oxidized GL/CCS ratio (w/w)	Particle size (nm)	Zeta potential (M_v)	Association efficiency (%)
0	183.6 ± 31.7[a]	34.5 ± 1.7	54.6 ± 2.5
0.07:1	114.3 ± 42.9[b]	12.2 ± 0.6	69.2 ± 3.8
0.14:1	127.4 ± 21.7[b]	9.3 ± 2.7	87.5 ± 2.3
0.28:1	369.5 ± 42.4[b]	3.4 ± 1.5	91.2 ± 4.1

[a]pH value of CCS-NPs suspension was 4.5. [b]pH value of CCS-NPs-GL suspension was 6.0.

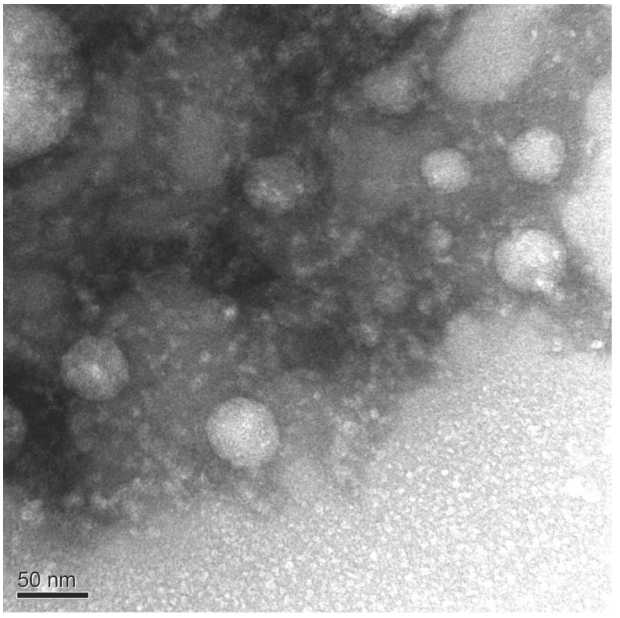

Figure 3. Transmission electron micrograph of CCS-NPs-GL prepared with oxidized GL/CCS ratio of 0.14:1 (w/w).

The morphological characteristic of nanoparticles is shown in Figure 3. The nanoparticles exhibited solid and discrete spherical shapes. It is noteworthy that the diameter of particles measured by DLS is higher than the size estimated from TEM particularly because of the high swelling capacity of CCS nanoparticles. Similar results were observed in the previous studies on chitosan nanoparticles[6,23]. The nanoparticles observed by TEM display lower values of diameter because of the drying of the sample suspension.

Nanoparticle stabilization and in vitro release of ADR from nanoparticles in plasma

The mean size of both CCS-NPs and CCS-NPs-GL in human plasma was measured at certain intervals. As shown in Figure 4a, the size of nanoparticles remained relatively stable during 0.5, 1, 2, 5, 12, and 24 hours, and surface GL-binding ratio of CCS-NPs-GL was at least 84.1% in fresh suspension and was retained to 67.6% after 24-hour exposure to the plasma (Figure 4b), which indicates that this nanoparticle system is stable in physiological condition and may be suitable for in vivo-targeting study.

To investigate the drug release characteristic of CCS-NPs-GL in plasma, ADR as a model drug was loaded into CCS-GL and CCS-NPs-GL prepared as above. As shown in Figure 5, ADR release profiles of two formulations were characterized by an initial increase and fast release period followed by a slower and stable release. The initial fast release of ADR is associated with those drug molecules dispersing close to the nanoparticle

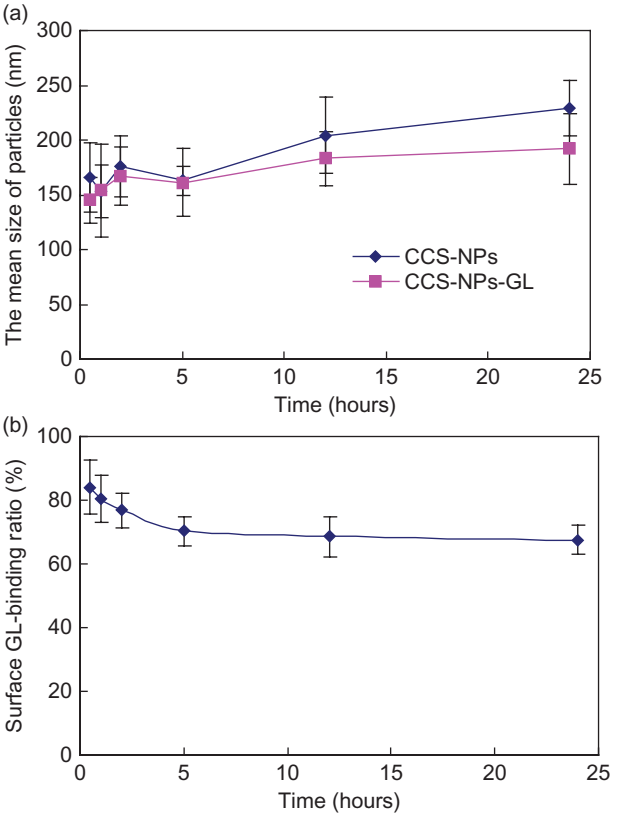

Figure 4. (a) Size alteration and stability of CCS-NPs and CCS-NPs-GL during 24 hours in human plasma in vitro. The size of nanoparticles was measured by dynamic light scattering (DLS), and the data were expressed by mean ± SD (n = 3); (b) Surface GL-binding stability of CCS-NPs-GL during 24 hours in human plasma in vitro. Glycyrrhetic acid, an aglycone of oxidized GL, hydrolyzed by 5% sulfuric acid was determined by HPLC. The data were expressed as mean ± SD (n = 3).

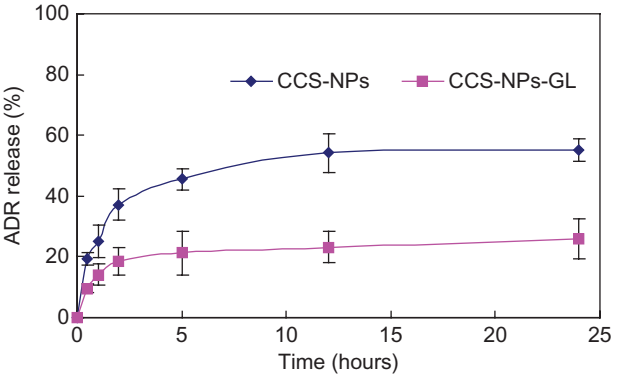

Figure 5. In vitro ADR release profiles of nanoparticles during 24 hours in plasma. ADR in plasma was measured by LC/MS/MS, and the data were expressed as mean ± SD (n = 3).

surface, which easily diffuse in the initial time. GL surface-modification made ADR more slowly to dissolve and diffuse to the plasma and led to lower extent of release. The slow release indicated that more ADR loaded into NPs can be distributed to special tissues, where drugs were released by either gradual disassembly or degradation of the nanoparticles[24].

In vivo tissue distribution of nanoparticles

TI of nanoparticles in different tissues was calculated, based on the $AUC_{(0-24)}$ for the various tissues, and was shown in Table 2. It was found that two nanoparticle formulations were accumulated in the liver and spleen. Of all the organs, the liver-TI of CCS-NPs-GL reached the highest level (TI = 5.83) and was nearly 1.6 times as high as the index of non-GL-modified CCS-NPs (TI = 3.54). Furthermore, the lung distribution of CCS-NPs-GL was significantly increased (TI = 2.29), indicating that CCS-NPs-GL had been targeted to the lung. In contrast to the increasing levels of ADR in the liver, spleen, and lung, the ADR distribution of CCS-NPs-GL in the heart and kidney was decreased (TI = 0.43 and 0.63, respectively), suggesting a limited potential for cardiac and renal damage.

The ADR distribution (expressed in μg/g tissues) in the liver was calculated in Figure 6. Following i.v. administration of ADR solution, CCS-NPs, and CCS-NPs-GL, the mean measured peak concentrations (1 hour after administration) were 18.9, 41.6, and 64.8 μg/g, respectively. It was obviously found that the nanoparticle

Table 2. Targeting evaluation after i.v. administration of F-ADR, ADR-loaded CCS-NPs, and CCS-NPs-GL in mice (n = 6).

	AUC_{0-t} (μg/mL·h or μg/g·h)		TI		
Tissue	F-ADR	CCS-NPs	CCS-NPs-GL	CCS-NPs	CCS-NPs-GL
Plasma	1.82	1.84	1.78	1.01	0.98
Heart	139.72	86.76	60.16	0.62	0.43
Liver	129.36	458.10	753.98	3.54	5.83
Spleen	783.97	4162.91	3322.32	5.31	4.24
Lung	77.02	135.37	176.13	1.76	2.29
Kidney	474.91	353.18	297.18	0.74	0.63

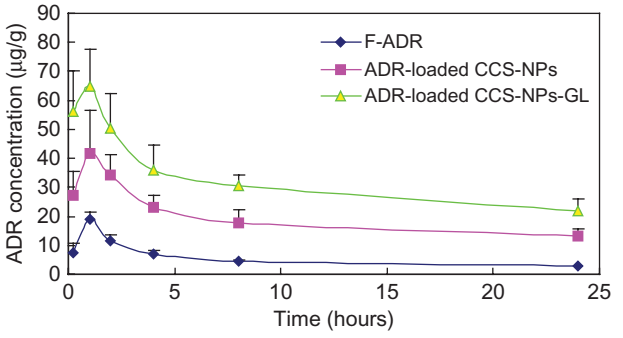

Figure 6. ADR concentration in liver at different times after i.v. administration of F-ADR, ADR-loaded CCS-NPs, and CCS-NPs-GL in mice, respectively (n = 6).

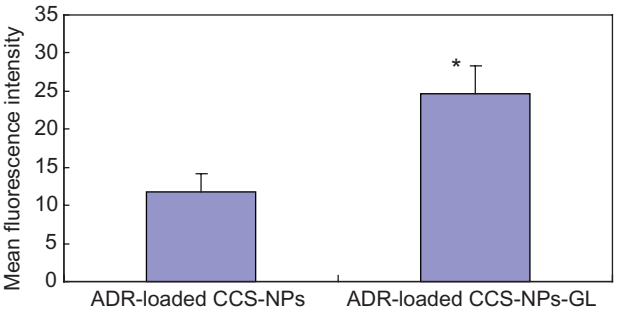

Figure 7. In vivo uptake of ADR-loaded CCS-NPs and CCS-NPs-GL in rat hepatocytes after 2 hours post-injection of two nanoparticle formulations. *$P < 0.05$ compared with CCS-NPs. Data were expressed as mean ± SD ($n = 3$).

formulations were more quickly accumulated in the liver, compared with the ADR solution. Furthermore, the ADR levels of CCS-NPs-GL in the liver were higher than those of non-GL-modified CCS-NPs during different times after administration.

In vivo hepatic cellular uptake of CCS-NPs-GL

To investigate whether hepatocytes take up more ADR-loaded CCS-NPs-GL than CCS-ADR, hepatocytes were isolated from rats after 1-hour post-injection of two nanoparticle formulations, and the mean fluorescence intensity in 5000 hepatocytes was detected by flow cytometry. The data are shown in Figure 7. It was found that the ADRs loaded into CCS-NPs-GL were significantly accumulated in hepatocytes ($P < 0.05$), and the amount of ADR loaded into CCS-NPs-GL in hepatocytes was 2.1 times as high as that in CCS-NPs, indicating that CCS-NPs-GL are preferentially distributed in hepatocytes by a ligand–receptor interaction.

Conclusion

In this study, we have focused on the characterization of CCS and (CCS-NPs-GL as a targeting drug delivery system to the liver. FTIR and ^{1}H-NMR spectroscopic analysis of synthetical product confirmed that the attachment of caproyl groups was through amino groups of chitosan. The CCS-NPs-GL formation was found to depend on the oxidized GL/CCS ratio (w/w). The nanoparticles using CCS molecules showed increased dimensional and GL surface-binding stability and slow release property in plasma in vitro, which suggest that hydrophobic caproyl groups can hinder hydrogen bonding and prevent aggregation. The results of tissue distribution study revealed that the CCS-NPs-GL are more efficiently accumulated in the liver compared with non-GL-modified CCS-NPs. Furthermore, more CCS-NPs-GL is taken up by the hepatocytes in the liver, which indicates that CCS-NPs-GL is a stable and suitable carrier for safe hepatocyte-targeting delivery.

Acknowledgment

This study was supported by the Natural Science Foundation of Guangdong Province, China (No. 04010047).

Declaration of interest: The authors report no conflicts of interest.

References

1. Torchilin VP. (2005). Fluorescence microscopy to follow the targeting of liposomes and micelles to cells and their intracellular fate. Adv Drug Deliv Rev, 57:95–109.
2. Stayton PS, Hoffman AS, Murthy N, Lackey C, Cheung C, Tan P, et al. (2000). Molecular engineering of proteins and polymers for targeting and intracellular delivery of therapeutics. J Control Release, 65:203–20.
3. Balthasar S, Michaelis K, Dinauer N, Von Briesen H, Kreuter J, Langer K. (2005). Preparation and characterisation of antibody modified gelatin nanoparticles as drug carrier system for uptake in lymphocytes. Biomaterials, 26:2723–32.
4. Aspden TJ, Mason JD, Jones NS, Lowe J, Skaugrud O, Illum L. (1997). Chitosan as a nasal delivery system: The effect of chitosan solutions on in vitro and in vivo mucociliary transport rates in human turbinates and volunteers. J Pharm Sci, 4:509–13.
5. Mao HQ, Roy K, Troung-Le VL, Janes KA, Lin KY, Wang Y. (2001). Chitosan-DNA nanoparticles as gene carriers: Synthesis, characterization and transfection efficiency. J Control Release, 70:399–421.
6. Aktaş Y, Andrieux K, Alonso MJ, Calvo P, Gürsoy RN, Couvreur P, et al. (2005). Preparation and in vitro evaluation of chitosan nanoparticles containing a caspase inhibitor. Int J Pharm, 298:378–83.
7. Chan P, Kurisawa M, Chung JE, Yang YY. (2007). Synthesis and characterization of chitosan-g-poly(ethylene glycol)-folate as a non-viral carrier for tumor-targeted gene delivery. Biomaterials, 28:540–9.
8. Kim TH, Nah JW, Cho MH, Park TG, Cho CS. (2006). Receptor mediated gene delivery into antigen presenting cells using mannosylated chitosan/DNA nanoparticles. J Nanosci Nanotechnol, 6:2796–803.
9. Jiang H-L, Kwon J-T, Kim Y-K, Kim E-M, Arote R, Jeong H-J, et al. (2007). Galactosylated chitosan-graft-polyethylenimine as a gene carrier for hepatocyte targeting. Gene Ther, 14:1389–98.
10. Mao SJ, Hou SX, Zhang LK, Wei DP, Bi YQ. (2005). Uptake of albumin nanoparticle surface modified with glycyrrhizin by primary cultured rat hepatocytes. World J Gastroenterol, 28:3075–9.
11. Negishi M, Irie A, Nagata N, Ichikawa A. (1991). Specific binding of glycyrrhetinic acid to the rat liver membrane. Biochim Biophys Acta, 1066:77–82.
12. Ismair MG, Stanca C, Ha HR, Renner EL, Meier PJ, Kullak-Ublick GA. (2003). Interactions of glycyrrhizin with organic anion transporting polypeptides of rat and human liver. Hepatol Res, 26:343–7.
13. Lin AH, Liu YM, Ping QN. (2007). Preparation and characterization of adriamycin-loaded chitosan nanoparticles surface-modified with glycyrrhizin. J China Pharm Uni, 38:507–11.
14. Lin AH, Liu YM, Ping QN. (2007). Studies of free amino groups on the surface of chitosan nanoparticles and its characteristics. Yao Xue Xue Bao, 42:323–8.

15. Lin AH, Liu YM, Huang Y, Sun JB, Wu ZF, Zhang X, et al. (2008). Glycyrrhizin surface-modified chitosan nanoparticles for hepatocyte-targeted delivery. Int J Pharm, 359:247–53.
16. Lee KY, Ha WS, Park WH. (1995). Blood compatibility and biodegradability of partially *N*-acylated chitosan derivatives. Biomaterials, 16:1211–6.
17. Lee DW, Powers K, Baney R. (2004). Physicochemical properties and blood compatibility of acylated chitosan nanoparticles. Carbohyd polym, 58:371–7.
18. Tien CL, Lacroix M, Ispas-Szabo P, Mateescu M. (2003). *N*-acylated chitosan: Hydrophobic matrices for controlled drug release. J control Release, 93:1–13.
19. Gupta PK, Hung CT. (1989). Quantitative evaluation of targeted drug delivery systems. Int J Pharm, 56:217–26.
20. Nguyen LT, Ishida T, Ukitsu S, Li WH, Tachibana R, Kiwada H. (2003). Culture time-dependent gene expression in isolated primary cultured rat hepatocytes by transfection with the cationic liposomal vector TFL-3. Biol Pharm Bull, 26:880–5.
21. Remant Bahadur KC, Aryal S, Bhattarai SR, Bhattarai N, Kim CH, Kim HY. (2006). Stabilization of gold nanoparticles by hydrophobically-modified polycations. J Biomater Sci Polym Ed, 17:579–89.
22. López-León T, Carvalho ELS, Seijo B, Ortega-Vinuesa JL, Bastos-González D. (2005). Physicochemical characterization of chitosan nanoparticles: Electrokinetic and stability behavior. J Colloid Interface Sci, 283:344–51.
23. Fernàndez-Urrusuno R, Calvo P, Remuñán-López C, Vila-Jato JL, Alonso MJ. (1999). Enhancement of nasal absorption of insulin using chitosan nanoparticles. Pharm Res, 16:1576–81.
24. Yu JJ, Lee HA, Kim JH, Kong WH, Kim Y, Cui ZY, et al. (2007). Bio-distribution and anti-tumor efficacy of PEG/PLA nanoparticles loaded doxorubicin. J Drug Target, 15:279–84.